# Chapter 5

# Fabrication and Characterization of InGaN Vertical Microcavity LEDs

## 5.1 Introduction

By introducing microcavity or photonic crystals, one can improve optical characteristics of an LED [8]. Vertical microcavity LEDs have advantages such as improved spectral purity or improved directionality, which provide higher efficiency of the light emitting devices. From the point of view of quantum information science and technologies, III-nitride microcavity micropillar or micropost, which is also a kind of DRB-based vertical-cavity emitters, is a promising candidate for the high-temperature high-efficiency single-photon emitter [116]. This aspect of nitride nanocavity light emitters is independently discussed in chapters 6 and 7. Nitride vertical-cavity surface emitting devices are also considered as a simple prototype of nitride VCSELs. As we described earlier in chapters 3 and 4, the author successfully achieved the growth of high reflectivity nitride n-type DBRs and several technological developments for the fabrication of nitride vertical-cavity surface emitting devices. In this chapter, successful fabrication of blue InGaN vertical microcavity LEDs with a Si-doped n-AlGaN/n-GaN DBR is demonstrated.

Magnetron-sputtered, transparent ITO film is employed as a p-contact. After the LED mesas is defined by $Cl_2$-based plasma etching, a 10.5 pairs of $SiO_2/ZrO_2$ top mirror is evaporated and wet-etched, followed by formation of an Al n-contact. EL spectra of these LEDs have reduced linewidth, exhibiting clear effects of microcavity. The angle dependence of the EL spectra reveals shift of main mode which can be reasonably explained by the angle dependence of the DBR resonance. Furthermore, directionality of the microcavity LED is dramatically improved to half angle of around 10 degree, compared to that of conventional one. The results are promising for

developing blue/ultraviolet VCSELs and high performance LEDs, as well as electrically-pumped single photon emitters.

## 5.2 Fabrication of InGaN Vertical Microcavity LEDs

All samples were grown on sapphire (0001) substrates by atmospheric pressure MOCVD. A Si-doped n-AlGaN/n-GaN DBR was grown on a 350-nm-thick nominally non-doped GaN layer. The Al composition of the n-AlGaN layer was estimated to be around 40 %. Even with such a high Al composition, sample surface exhibited good morphology and no cracks were observed all over the wafer. Considering uniformity and optical bandwidth of the mirror, a 26-period n-type DBR (measured maximum reflectivity was 91 % at $\lambda$ = 400 nm) was employed. Extremely high reflectivity of bottom DBR, which is essential for VCSEL application, is not always necessary for MCLEDs. The DBR was characterized by high-resolution X-ray diffraction analysis, optical reflectance spectroscopy, and Hall measurement. On top of the DBR, a 3-$\lambda$-length cavity including an active region consists of five $In_{0.08}Ga_{0.92}N/In_{0.03}Ga_{0.97}N$ multiple-quantum-wells was grown. The active region was grown at 750 °C with $NH_3$, $H_2$, and $N_2$ flow rates of 10.0, 0.20, and 12.5 slm, respectively, while Mg-doped GaN was grown at 1045 °C with $NH_3$, $H_2$, and $N_2$ flow rates of 3.0, 4.0, and 35.0 slm, respectively. Special care was taken to match the three characteristic wavelengths, i.e., the SL-DBR stop-band, the InGaN emission peak, and the cavity resonance. After the growth, rapid thermal annealing was performed under nitrogen ambient for 5 minutes at 1000 °C in order to activate acceptors in the Mg-doped GaN. Carrier concentration of the resultant p-GaN layer was estimated to be around $8.0 \times 10^{17}$ $cm^{-3}$.

Figure 5.1 shows the schematic structure of the fabricated LED. Figure 5.2 is a plan-view image of the fabricated device. Listed in Table 5.1 are the detail procedures and conditions practically used for the fabrication of the device. We had improved and optimized the procedures and conditions thereafter. Hence Figure 5.3 illustrates the optimized process flow, which listed in detail in Table 5.2. In this study, transparent ITO was employed as a p-type ohmic contact material. A 50-nm-thick magnetron sputtered ITO thin film was deposited on the sample and annealed at 600°C under nitrogen ambient to reduce contact resistance and increase transparency. Over 90 % of transmittance at $\lambda$ = 400 nm was obtained after this annealing, as described in chapter 4. LED mesas were defined by $Cl_2$-based inductively coupled plasma reactive ion etching (ICP-RIE) with Ni as a mask material. Note that a Ni mask has superior properties as an etching mask for III-nitride semiconductors. First,

it can serve good selectivity for the $Cl_2$-based RIE of nitrides. The selectivity for GaN etching is approximately 8 times, which is much higher than that of $SiO_2$ (~ 4 times) or photoresists (almost the same or even less). Secondly, Ni can be removed by $H_3PO_4$-based solution (Al-etchant) with underlying ITO remain unetched. This feature is especially favorable since, as can be seen the process flow (Fig. 5.3, Tables 5.1 and 5.2), a self-aligned top-contact of the LED mesas can be formed by a simple method. After formation of the mesas, a 10.5-period $SiO_2/ZrO_2$ top mirror (measured reflectivity over 99.5% at $\lambda$ = 400±10 nm) was evaporated on top of them. Standard photolithography using AZ1500(20cp) diluted with the same volume of OFPR thinner was employed to pattern the top mirror. Finally, an Al n-contact was deposited on the etched n-DBR surface.

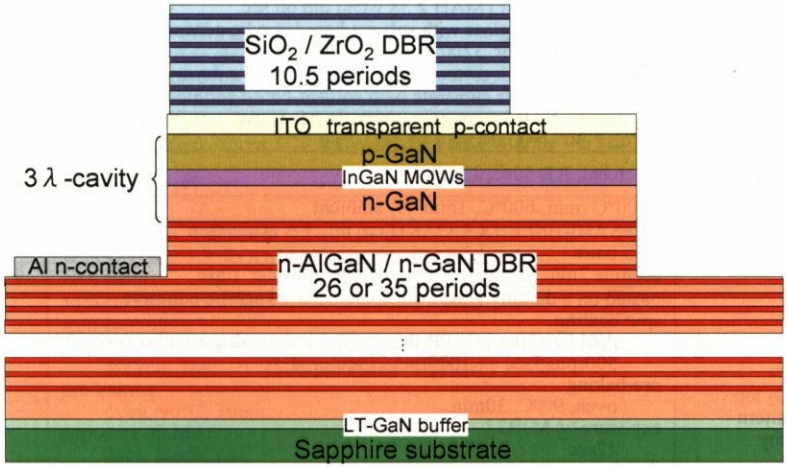


Figure 5.1 Schematic structure of fabricated microcavity LED

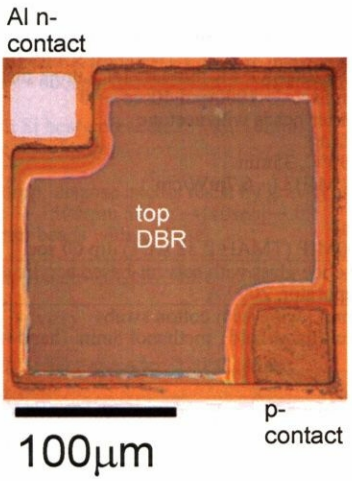


Figure 5.2 Microscope plan-view image of a fabricated microcavity LED

| | Procedure | Conditions | Remarks |
|---|---|---|---|
| 1 | Mg activation anneal | +630°C /min, 1000°C, 5min. $N_2$ ambient | |
| 2 | degrease | acetone 5min. methanol 5min. deionized water. 5min. US, deionized water rinse | |
| 3 | ITO sputtering | pasted on a 2" glass plate with solvent-based acrylic adhesive<br>ULVAC SOLCIET, Ar 11.7sccm, $O_2$ 0.12sccm, 400W, ~2'30"(=50nm) | |
| 4 | cleavage | 4mm × 4mm | |
| 5 | mesa pattern lithography | pasted on a dummy glass with solvent-based acrylic adhesive<br>spin coating<br>AZ1500(20cp):OFPR thinner=1:1 a drop, dispose excess resist by gravity<br>500rpm 5sec → 800rpm 40sec →[10sec]→ 0<br>wipe out corner beads with acetone<br>pre-baking<br>oven, 90°C, 30min.<br>exposure @ MJB3 (~ 6.7mW/cm$^2$)<br>12sec<br>development<br>AZ 300MIF (TMAH 2.38 wt%) dip 120 sec.<br>exposure 2nd for better patterning @ MJB3 (~ 6.7mW/cm$^2$)<br>12sec<br>development 2nd<br>AZ 300MIF (TMAH 2.38 wt%) dip 60 sec. | |
| 6 | Ni mask-metal deposition | pasted on a slide glass with solvent-based acrylic adhesive<br>thermal evaporator, 3200 Å | |
| 7 | Ni lift off | acetone, wipe with cotton swabs tenderly → no extensive cleaning → $N_2$ blow | |
| 8 | RIE | pasted on the glass substrate with solvent-based acrylic adhesive<br>$Cl_2$ 3sccm, Xe 0.3sccm, ICP 300W, BIAS 100W, 1.80Pa→0.50Pa, He $7.0\times10^2$Pa<br>50°C, 7'30" (= GaN 5'30" + ITO 2'00") | |
| 9 | Ni etching | Al etchat, RT, 50cc, 13min | 4min. was enough |
| 10 | ITO anneal | +600°C /min, 600°C, 1min. $N_2$ ambient | |
| 11 | $ZrO_2/SiO_2$ coating | @ ASAHI-BEER KOUGAKU co. ltd., EB evaporator<br>10.5 pairs | conditions undisclosed |
| 12 | degrease | acetone 3min, methanol 3min, deionized water. rinse | hand-shook |
| 13 | $ZrO_2/SiO_2$ top mirror pattern lithography | pasted on a dummy glass with solvent-based acrylic adhesive<br>spin coating<br>AZ1500(20cp):OFPR thinner=1:1 a drop, dispose excess resist by gravity<br>500rpm 5sec → 1000rpm 20sec → 0<br>pre-baking<br>oven, 90°C, 30min.<br>exposure @ MJB3 (~ 6.7mW/cm$^2$)<br>12sec<br>development<br>AZ 300MIF (TMAH 2.38 wt%) dip 60 sec.<br>post-baking<br>oven, 120°C, 30min | |
| 14 | $ZrO_2/SiO_2$ etching | BHF, RT, 1min. + 15sec. + 5sec. | |
| 15 | resist removal, $ZrO_2$ residue removal | acetone, wipe with cotton swabs | swab pressed |
| 16 | n-contact pad pattern lithography | pasted on a dummy glass with solvent-based acrylic adhesive<br>spin coating<br>AZ1500(20cp):OFPR thinner=1:1 a drop, dispose excess resist by gravity<br>500rpm 5sec → 1000rpm 40sec → 0<br>wipe out corner beads with acetone<br>pre-baking<br>oven, 90°C, 35min.<br>exposure @ MJB3 (~ 6.7mW/cm$^2$)<br>12sec<br>development<br>AZ 300MIF (TMAH 2.38 wt%) dip 60 sec. | 30min was enough for pre-baking |
| 17 | Al contact deposition | pasted on a slide glass with solvent-based acrylic adhesive<br>thermal evaporator, 2000 Å | |
| 18 | Al lift off | acetone 10min., wipe with cotton swabs<br>acetone 5min (hand-held), methanol 5min. (hand-held) US, deionized water rinse → $N_2$ blow | conditions note recorded |

Table 5.1. process procedures and their conditions for MCLED fabrication

| | Procedure | Conditions | Remarks |
|---|---|---|---|
| 1 | Mg activation anneal | +630°C /min, 1000°C, 5min. $N_2$ ambient | |
| 2 | degrease | acetone 5min. methanol 5min. deionized water. 5min. US, deionized water rinse | |
| 3 | ITO sputtering | pasted on a glass plate with GEL-FILM<br>Ar 10sccm, $O_2$ 0.1sccm, 50W, 3'08"(=50nm), HALF | |
| 4 | ITO anneal | +800°C /min, 800°C, 5sec. $N_2$ ambient | |
| 5 | mesa pattern lithography | spin coating<br>AZ1500(20cp):OFPR thinner=1:1 1 drop, dispose excess resist by gravity<br>500rpm 5sec → 800rpm 2sec →[5sec]→ 4000rpm, 40sec → 0<br>hard-baking<br>hot-plate with Si heat-spreader, 135°C, 10min.<br>cooling more than 5min.<br>spin coating<br>AZ5206E 1 drop, dispose excess resist by gravity<br>500rpm 5sec → 1500rpm 50sec →[10sec]→ 0<br>wipe out corner beads with acetone<br>pre-baking<br>hot-plate with Si heat-spreader, 90°C, 60sec.<br>exposure @ MA6<br>1.7sec, mode:HARD<br>reversal baking<br>hot-plate with Si heat-spreader, 120°C, 45sec.<br>flood exposure @ MA6<br>28.6mW/cm2, 69.9sec, (=2J/cm$^2$) mode:FLOOD-E<br>development<br>NMD-3 (TMAH 2.38 wt%) dip 30 sec. | |
| 6 | Ni mask-metal deposition | pasted on a slide glass with GEL-FILM<br>EB evaporator, 5Å/s, 1500 Å | |
| 7 | Ni lift off | acetone, a few minutes → mild cleansing by US → $N_2$ blow | |
| 8 | RIE | pasted on the glass substrate with GEL-FILM<br>$Cl_2$ 3sccm, Xe 0.3sccm, ICP 300W, BIAS 100W, 1.80Pa→0.50Pa, He 7.0×$10^2$Pa<br>50°C, 3'00" (?) | |
| 9 | Ni etching | Al etchat, RT, 50cc, 5min | |
| 10 | cleaning | acetone 5min., methanol 5min., US, deionized water rinse → $N_2$ blow | |
| 11 | $ZrO_2/SiO_2$ coating | @ ASAHI-BEER KOUGAKU co. ltd., EB evaporator<br>10.5 pairs | conditions undisclosed |
| 12 | degrease | acetone 3min, methanol 3min, deionized water. rinse | hand-shook |
| 13 | $ZrO_2/SiO_2$ top mirror pattern lithography | spin coating<br>AZ1500(20cp):OFPR thinner=1:1 1 drop, dispose excess resist by gravity<br>500rpm 5sec → 2500rpm 40sec →[10sec] → 0<br>pre-baking<br>oven, 90°C, 30min.<br>exposure @ MA6<br>2sec, mode:VAC<br>development<br>NMD-3 (TMAH 2.38 wt%) dip 10 sec.<br>post-baking<br>oven, 120°C, 30min | |
| 14 | $ZrO_2/SiO_2$ etching | BHF, RT, 1min. | |
| 15 | resist removal, $ZrO_2$ residue removal | acetone, wipe with cotton swabs | swab pressed |
| 16 | n-contact pad pattern lithography | spin coating<br>AZ1500(20cp):OFPR thinner=1:1 1 drop, dispose excess resist by gravity<br>500rpm 5sec → 800rpm 2sec →[5sec]→ 4000rpm, 40sec → 0<br>hard-baking<br>hot-plate with Si heat-spreader, 135°C, 10min.<br>cooling more than 5min.<br>spin coating<br>AZ5206E 1 drop, dispose excess resist by gravity<br>500rpm 5sec → 1500rpm 50sec →[10sec]→ 0<br>wipe out corner beads with acetone<br>pre-baking<br>hot-plate with Si heat-spreader, 90°C, 60sec.<br>exposure @ MA6<br>1.7sec, mode:HARD<br>reversal baking<br>hot-plate with Si heat-spreader, 120°C, 45sec.<br>flood exposure @ MA6<br>28.6mW/cm2, 69.9sec, (=2J/cm$^2$) mode:FLOOD-E<br>development<br>NMD-3 (TMAH 2.38 wt%) dip 30 sec. | |
| 17 | Al contact deposition | pasted on a slide glass with GEL-FILM<br>EB evaporator, 2000 Å | |
| 18 | Al lift off | acetone, a few minutes → mild cleansing by US, deionized water rinse → $N_2$ blow | |

Table 5.2. an ideal process procedures and their conditions for MCLED fabrication

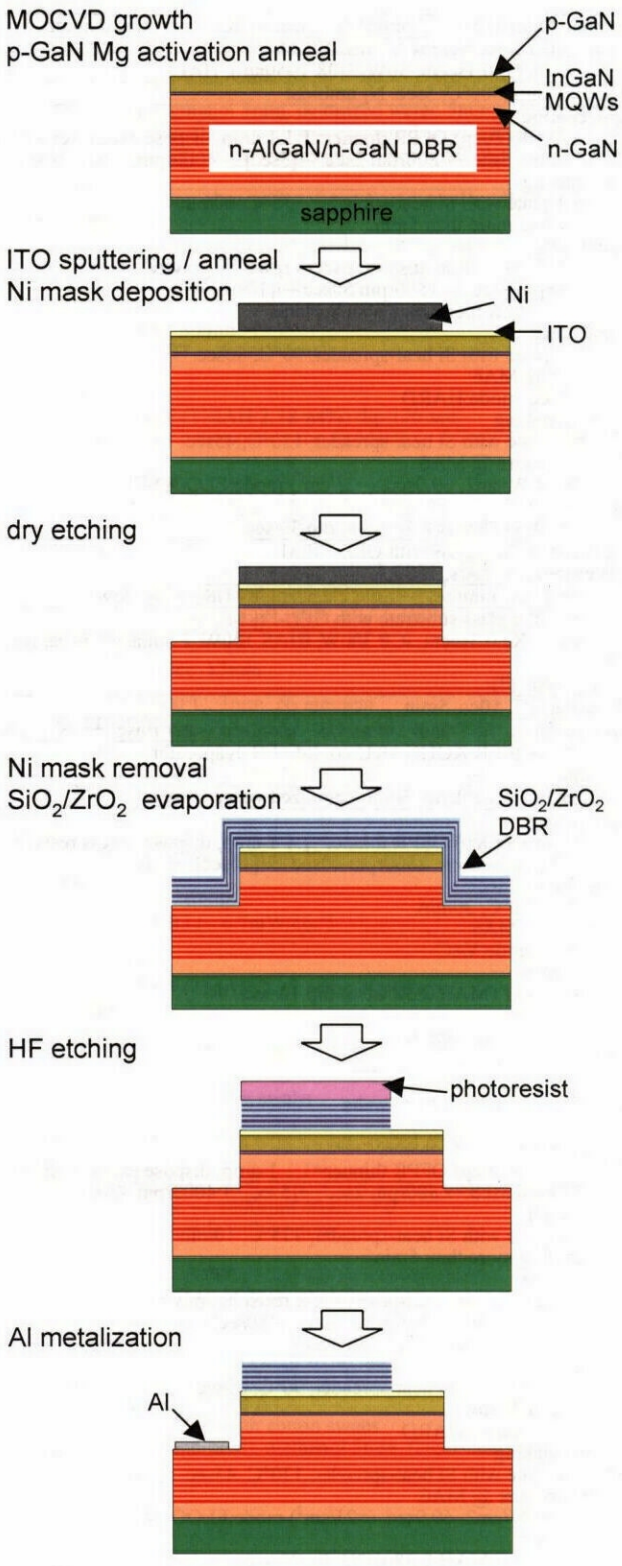


Figure 5.3 Process flow of a microcavity LED

## 5.3 Characterization of InGaN Vertical Microcavity LEDs

### 5.3.1 Optical Properties

Before processing, reflectivity and photoluminescence (PL) spectra were measured at room temperature. Reflectivity was measured using Xe lump as a light source, while PL was measured under He-Cd laser excitation. The results are shown in Figure 5.4. Even without top high-reflectivity mirror, narrow PL peak corresponding the cavity mode was clearly seen. At this stage, air / p-GaN interface was served as a mirror with reflectivity of approximately 19 %. The cavity mode was appeared as a dip in the reflectivity spectrum. Slight discrepancy of the mode wavelength between the two spectra is due to nonuniformity of the sample wafer and the different size of detecting spot. For PL, the excitation spot was focused within the region of which diameter was well below 500 μm. Because of the limitation of our experimental setup, the reflectivity signals from rather large ($\phi \sim$ 1mm) area was integrated and detected.

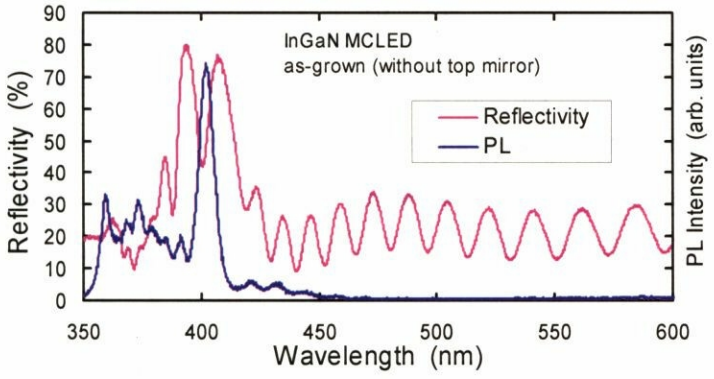


Figure 5.4 Reflectivity and PL spectra of the as-grown (unprocessed) MCLED structure

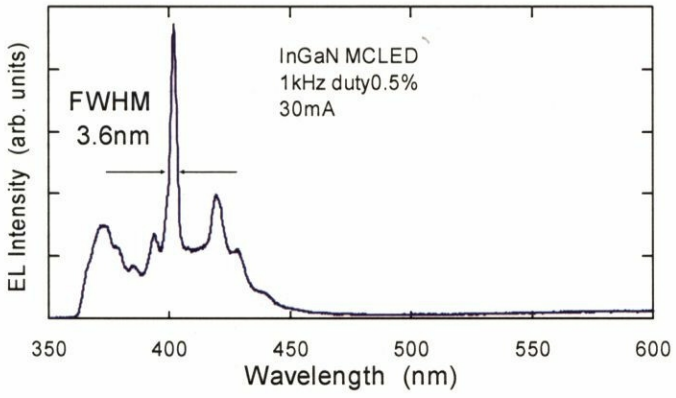


Figure 5.5 EL spectrum of the fabricated MCLED

After the process was completed, Electroluminescence (EL) spectra were measured at room temperature. With a high reflectivity mirror coated atop, EL emission was detected from backside, i.e. through the sapphire substrate. In Figure 5.5, the EL spectrum of the fabricated MCLED under the excitation condition of 1kHz with 0.5 % duty and peak current of 30 mA, is shown. The peak emission width was reduced to 3.6 nm, which gave the estimation of the cavity $Q$ value of about 110. Note that a standard (without microcavity) LED with similar InGaN multi-quantum-wells active layer, fabricated for comparison, exhibited EL linewidth of 12 nm. The other two peaks observed in Figure 5.5, at $\lambda$ = 374 nm and 420 nm, are the spectral modulations due to stop-band width of the nitride DBR. In addition, the emission angle dependence of EL spectra revealed blue shift of the main mode with increasing off-axis angle because DBR resonance peak also shifted toward the shorter wavelength as shown in Figure 5.6. Detection angle was varied with 5° step. The peak wavelength is plotted in Figure 5.7. A theoretical curve derived from the equation,

$$\frac{\lambda_\theta}{\lambda_0} = \sqrt{1-\left(\frac{\sin\theta}{n}\right)^2} \tag{5.1}$$

is also given on the graph. Here, $\lambda_0$ means the wavelength at the normal incidence, $\lambda_\theta$ means resonance wavelength at the incidence angle $\theta$, $n$ is the refractive index of the medium. As $n$ being the variable parameter, fitting to the experimental data resulted in $n$ = 2.54, which is quite close to the refractive index of GaN [90]. This is another evidence that the observed peak comes from resonance in the microcavity.

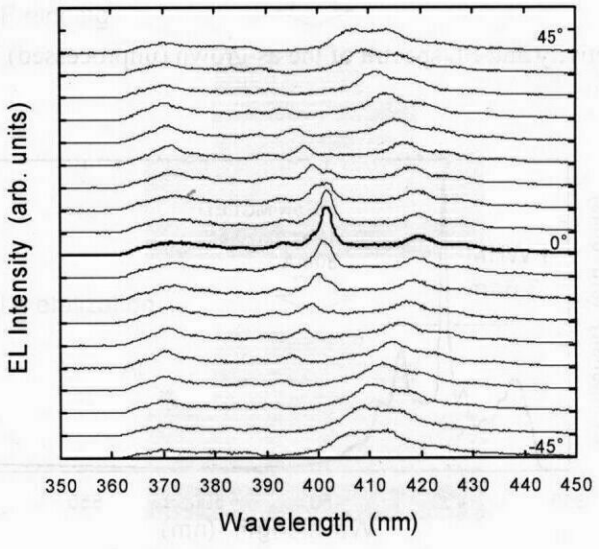


Figure 5.6 Angle dependent EL spectra of the microcavity LED

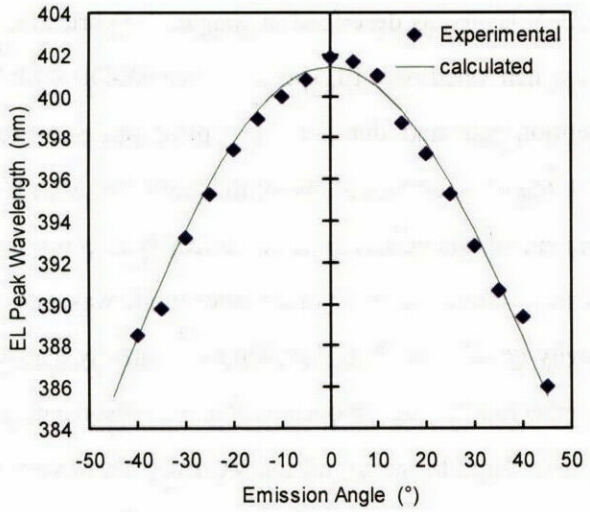


$$\frac{\lambda_\theta}{\lambda_0} = \sqrt{1-\left(\frac{\sin\theta}{n}\right)^2}, \qquad n_{GaN} = 2.54$$

Figure 5.7 Analysis of angle dependence of the EL peak wavelengths

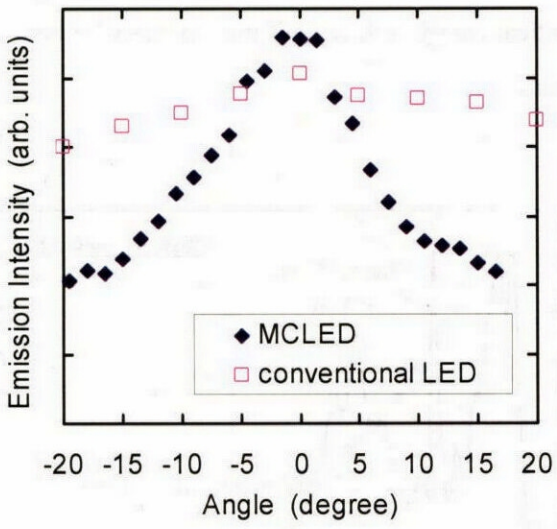


Figure 5.8 Directionality (far field patterns) of microcavity LED and conventional LED

Figure 5.8 shows far field patterns of the fabricated device and a conventional LED. irectionality of the MCLED was dramatically improved to around 10° (half angle), compared to at of conventional one. These optical characteristics are clear evidences of microcavity effects.

For further improvement, superlattice layers were introduced in the nitride DBR instead of single quarter-wave n-AlGaN layers, as described in chapter 3. Fabrication procedures were almost the same as the previously-mentioned one. EL spectra of the SL-DBR MCLEDs were measured at room temperature. Repetition rate and duration of applied pulses were 1 kHz and 500 nsec, respectively. In Figure 5.9, the EL spectrum of one of the fabricated MCLED is shown. Peak current was 40 mA at this experiment. As can be seen, clear microcavity effects due to cavity resonance have been observed. The emission width of the cavity resonance mode was measured to be 3.0 nm, which gave estimation of the cavity $Q$ value of about 130. Due to relatively narrow stop-band width of the nitride SL-DBR, there appeared leakage modes beside the resonance mode. Evidently, higher reflectivity for the DBR is required to realize nitride VCSELs. However, by utilizing the SL-DBR, series resistance of MCLEDs was improved to be roughly half as those of conventional ones as described below. We can expect, then, the SL-DBR will be a promising structure for successful fabrication of current-injected nitride vertical-cavity surface-emitting devices. On the other hand, Mg-doped AlGaN/GaN short-period superlattice, in which acceptor activation is enhanced due to polarization [117], is now considered to be one of the most practical schemes for hole conductive layer in nitride-based ultra-violet optoelectronic device applications [118]. Therefore, it is reasonable to expect that all-nitride vertical-cavity surface emitting devices with both p-type and n-type SL-DBRs will be realized in the future.

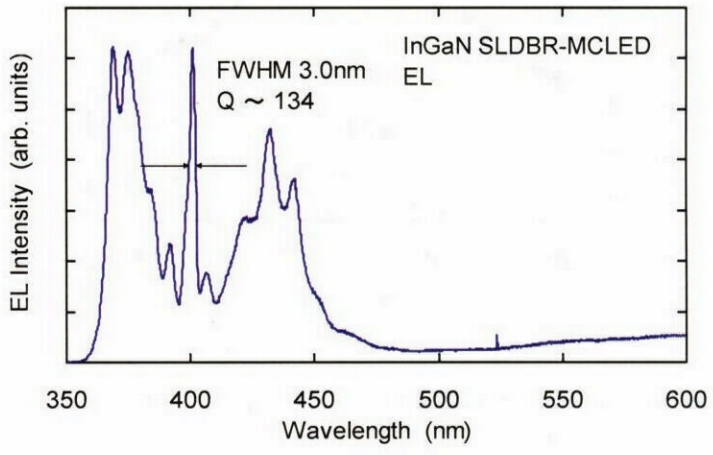


Figure 5.9 EL spectrum taken from a MCLED with a superlattice DBR

### 5.3.2 Electrical Properties

As for the ITO p-contact, it is confirmed from fundamental characteristics of the devices that the contact embedded in the cavity efficiently supplied carriers beneath the dielectric mirror. Otherwise, the cavity resonance mode should not be observed in EL spectrum. We also observed that hole current spread homogeneously all over the contact area (0.34 $mm^2$). The specific contact resistance has not been measured yet, but we believe this transparent electrode will be useful for the III-nitride vertical microcavity light emitting devices.

Figure 5.10 shows current-voltage (I-V) characteristics of both the MCLED with a normal n-DBR and the modified MCLED with SL-DBR. Both devices were grown with 26-pair nitride n-DBR. Reduction in series resistance in the latter device was observed. As etching conditions have not been optimized yet, plasma-etched n-DBR/contact interface resistance may greatly affect the total resistance of the final devices. For further reduction of series resistance, plasma etching conditions and n-DBR doping profiles should be optimized. Although the MCLEDs had relatively high series resistance, it is worth mentioning that vertical electrical conductance across the n-type nitride DBR was successfully demonstrated, which proves its potential for nitride VCSEL application.

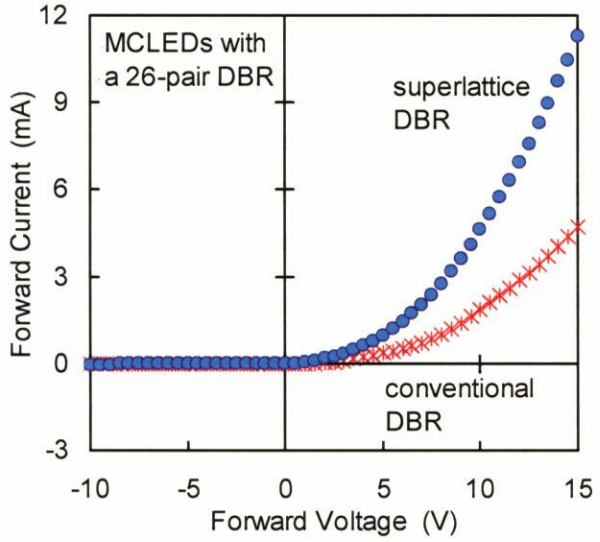


Figure 5.10 I-V characteristics of microcavity LEDs with a 26-pair nitride DBR

## 5.4 Prospects for Nitride Vertical-Cavity Surface-Emitting Lasers

After the first proposal of nitride blue vertical-cavity surface-emitting lasers [12], several groups have reported theoretical studies on design of the devices. Honda et al. estimated threshold current density in GaN-based VCSELs by means of density matrix method taking into account intraband relaxation lifetime and indicated that quantum-well-based active region is effective for low threshold current operation [119]. On the other hand, Mackowiak et al. at Lodz institute of technology have analyzed threshold current density of nitride VCSELs taking into account various loss factors and have concluded that bulk active region rather than quantum well provides us more flexibility from the viewpoint of device design [120]. Here, nitride VCSEL threshold current density is roughly estimated using experimentally deduced gain factor in the InGaN quantum well active regions.

Our group has already succeeded in optical-pumped operation of nitride VCSELs. Someya et al. investigated input-output characteristics and estimated threshold carrier density per an $In_{0.1}Ga_{0.9}N$ quantum well [16]. According to their calculation, the threshold carrier density $N_{th}$ per a quantum well is approximately $2\sim4\times10^{12}$ $cm^{-2}$, with the sample structure of dielectric DBR ($R \sim 99.5$ %) and nitride DBR ($R \sim 98$ %). Assuming that the cavity with equivalent optical or structural quality can be made and additional losses due to impurity doping inside the whole structure are negligible, we estimated threshold current density of a nitride VCSEL.

Relation between threshold carrier density $N_{th}$ and threshold current density $J_{th}$ is given as follows:

$$J_{th} = \frac{e}{\eta_i \tau_s} n N_{th} \tag{5.2}$$

where $n$ stands for the number of quantum well active layers. Also $\eta_j$ is injection efficiency with which carriers are injected into active region, and becomes smaller when there is leakage current or carrier overflow. $\tau_s$ is carrier lifetime, $e$ is charge of an electron. Considering five quantum wells are embedded in the cavity, $\eta_j$ can be regarded as approximately 1 for every quantum well. If recombination rate for the carriers is estimated around 1 ns, threshold current density $J_{th}$ can be calculated to be 1.6~3.2 $kA/cm^2$. For further investigations, we assume that our VCSEL structure has post-like vertical cavity of diameter of 30 μm, and that all of the currents can contribute radiative recombination inside the active region. Then, the threshold current $I_{th}$ becomes 11~23 mA. Effective diameter of the cavity can be reduced by applying appropriate current confinement structure. Very recently, successful oxidization scheme of AlGaN layers have been reported to fabricate oxide

confinement structure in nitride vertical-cavity devices [121]. Of course, this estimation might be underestimate the threshold current, because there are various factors increasing threshold current in practical structure such as leakage current paths or nonradiative recombination processes. However, it is still encouraging result that reasonable threshold current will be achieved with presently achievable quality of nitride DBRs.

As we discussed in chapter 3, VCSEL requires very high reflectivity mirrors. We have already grown high reflectivity n-AlGaN/n-GaN DBRs. A similar but undoped DBR was used to achieve optically-pumped lasing operation of nitride VCSEL [16]. Considering that theoretical analysis has revealed the possibility of obtaining electrical conductivity when high-quality nitride DBRs with high doping concentration ($\sim 10^{19}$ $cm^{-3}$) can be grown, sufficiently low resistivity for lasing operation will be achieved by improving the crystalline quality of nitride n-DBRs. Recent progress in high-quality Al(Ga)N growth by modifying the initial growth conditions is promising [105]. From the viewpoint of device fabrication, we have developed several technologies useful for VCSEL fabrication processes. If we can obtain much lower resistance of the vertical cavity devices, it can be expected that one can realize nitride VCSEL in the near future. As Nakwaski et al. pointed out, structural parameters should be carefully optimized to construct the nitride-based blue VCSELs [82]. If the major problem to be overcome is electrical characteristics of the hybrid cavity, not only the electrical properties of n-DBRs but also contact resistances should be improved. Contact resistance of n-GaN/metal interface can be improved by careful optimization of process procedures. RIE condition which directly influence structural properties of the n-GaN surface and surface preparation techniques prior to deposition of the metal are to be optimized. Post-deposition annealing of the metal contact can reduce the contact resistance greatly, but in the same time it can degrade other parts of the devices. One must take special care not to damage the device in fabrication process.

## 5.5 Summary

We have achieved current injection through the n-AlGaN/n-GaN DBR in blue InGaN vertical MCLEDs with their fundamental light emission properties. Electrically conductive n-type DBRs with high reflectivity have been obtained through precise control of growth conditions. A transparent ITO electrode has been used for hole spreading layer. EL measurement has shown narrower peak width and improved directionality, which are clear evidences of microcavity effects. Furthermore, superlattice DBRs were proved to be effective to improve the electrical properties of the devices.

Prospects for further progress toward current-driven nitride VCSEL were discussed. The results are promising for developing VCSELs and high performance LEDs.